

1
2
3
4 **Light management design in ultra-thin chalcopyrite photovoltaic devices by employing**
5 **optical modelling**
6
7

8
9 M. Kovacic¹, J. Krc¹, B. Lipovsek¹, W-C Chen², M. Edoff², P.J. Bolt³, J. van Deelen³, M. Zhukova⁴,
10 J. Lontchi⁴, D. Flandre⁴, P. Salomé⁵ and M. Topic¹
11

12 ¹University of Ljubljana, Faculty of Electrical Engineering, Trzaska 25, 1000 Ljubljana, Slovenia

13 ²Uppsala University, dep. Eng. Sciences, Angstrom lab, p.o. box 534, 751 21 Uppsala, Sweden

14 ³TNO, Solar Technology and Applications, High Tech Campus 21, 5656 AE Eindhoven, The Netherlands

15 ⁴Université catholique de Louvain, ICTEAM institute, Place du Levant 3, 1348 Louvain-la-Neuve,
16 Belgium
17

18 ⁵International Iberian Nanotechnology Laboratory 4715-330 Braga, Portugal
19 (corresponding author; Milan Kovacic, E-mail: milan.kovacic@fe.uni-lj.si)
20
21

22 **Abstract**
23

24 In ultra-thin chalcopyrite solar cells and photovoltaic modules, efficient light management is
25 required to increase the photocurrent and to gain in conversion efficiency. In this work we
26 employ optical modelling to investigate different optical approaches and quantify their potential
27 improvements in the short-circuit current density of Cu(In, Ga)Se₂ (CIGS) devices. For structures
28 with an ultra-thin (500 nm) CIGS absorber, we study the improvements related to the
29 introduction of (i) highly reflective metal back reflectors, (ii) internal nano-textures applied to the
30 substrate and (iii) external micro-textures by using a light management foil. In the analysis we
31 use CIGS devices in a PV module configuration, thus, solar cell structure including encapsulation
32 and front glass. A thin Al₂O₃ layer was considered in the structure at the rear side of CIGS for
33 passivation and diffusion barrier for metal reflectors. We show that not any individual
34 aforementioned approach is sufficient to compensate for the short circuit drop related to ultra-thin
35 absorber, but a combination of a highly reflective back contact and textures (internal or external)
36 is needed to obtain and also exceed the short-circuit current density of a thick (1800 nm) CIGS
37 absorber.
38
39
40
41
42
43
44
45
46
47
48
49
50
51
52
53
54
55
56
57
58
59
60
61
62
63
64
65

1
2
3
4 **Keywords:** ultra-thin chalcopyrite solar cells, light management, reflector, textures, optical
5
6 modelling
7
8

9 10 **1. Introduction**

11
12 Among thin-film solar cell technologies, Cu(In, Ga)Se₂ (CIGS) solar cells exhibit high
13 conversion efficiencies, with a recent record of 23.35% on the cell level [1] and 19.2 % on PV
14 module level [2]. Different approaches have been taken to increase efficiencies, such as
15 optimized Ga grading in the CIGS absorber, application of different buffer layers (such as ZnS,
16 Zn(O,S) or ZnSe), a combination of different post-deposition treatments (e.g. by potassium
17 fluoride, by sodium fluoride etc.) and others [3]. The CIGS alloy is a direct semiconductor
18 material, enabling high optical absorption which is beneficial for thin-film technology. Still, a
19 thickness of the CIGS layer around 2 μm is used for sufficient absorption of long-wavelength
20 light. In order to minimize the material consumption, especially the use of the scarce metals
21 indium and gallium [4,5], to speed up the fabrication process and hence to lower the cost, further
22 thinning down of CIGS absorber layer is important [6–9]. Ultra-thin (thickness $d_{\text{CIGS}} < 500$ nm)
23 CIGS cells with graded absorber and efficiency over 15 % have already been demonstrated [10].
24 Two of the challenges related to the use of thin absorber layer are the pronounced impact of
25 charge carrier surface recombination (affecting the voltage and fill factor of the device) and
26 decreased photocurrent. To mitigate the effect of reduced voltage, efficient surface passivation
27 has to be ensured. Thin passivation layers, such as Al₂O₃ have been applied to the rear CIGS/Mo
28 interface [11–14]. To compensate for reduced photocurrent, an additional treatment to increase
29 light absorption in the thin absorber needs to be carried out. Different solutions have been
30 reported to increase the short-circuit current density (J_{sc}), focusing on various aspects, from
31 improving front transparent contacts [15–17], using alternative window layers [18,19],
32
33
34
35
36
37
38
39
40
41
42
43
44
45
46
47
48
49
50
51
52
53
54
55
56
57
58
59
60
61
62
63
64
65

1
2
3
4 implementing anti-reflecting structures [20], inclusion of efficient back reflectors [21,22],
5
6 introduction of textures and nano-particles to induce light scattering [23–28]. A review on light
7
8 management in thin CIGS is given in [29].
9

10
11 In this paper, we employ optical simulations to determine the potential improvements in J_{sc} of
12
13 CIGS devices with 500 nm thick absorber layer, related to the introduction of (i) highly reflective
14
15 metal back reflectors, (ii) internal nano-textures and (iii) external micro-textures by applying a
16
17 light management (LM) foil. In simulations with experimentally-calibrated optical models, we
18
19 consider not only layers forming the solar cell structure, but also take into account encapsulation
20
21 and front glass, as in final PV module realizations. The encapsulation changes optical conditions
22
23 at the front side (light in-coupling), therefore, it is important to consider the complete, final
24
25 device structure in the optimization process [23]. We investigate different metal materials in the
26
27 role of back reflectors in simulations, namely copper (Cu), aluminum (Al) and silver (Ag). A thin
28
29 Al_2O_3 layer is used on top of these metallic layers, assuming not only its function of passivation
30
31 of the CIGS rear surface, but also serving as a sufficient diffusion barrier for metals, mitigating
32
33 their diffusion in the CIGS layer during the evaporation process. We show that in thin devices,
34
35 high optical reflection at the back reflector is not sufficient to reach the J_{sc} of the reference device
36
37 with 1800 nm thick CIGS layer and Mo contact, but needs to be combined with other measures
38
39 such as internal or external textures. This way we can reach and outperform the efficiency of
40
41 standard thick devices with thinner ones.
42
43
44
45
46
47
48
49
50
51
52

53 **2. Modelling**

54
55 Modelling and simulations enable us to analyze, predict and optimize devices behavior prior to,
56
57 or in parallel with, experimental work. Optical simulations of devices in this paper were carried
58
59
60
61
62
63
64
65

1
2
3
4 out with models that have been verified and described in more detail in previous publications
5
6 [30–34], thus, here we only provide their brief descriptions. We will also explain the electrical
7
8 assumptions that we consider for the determination of device external parameters, namely the
9
10 external quantum efficiency (EQE) and J_{sc} from the results of optical simulations.
11
12
13
14
15
16
17

18 **2.1 Simulation tools**

19
20
21 Three different optical simulators have been used for analysis and optimization of thin CIGS
22
23 devices. Firstly, one-dimensional semi-coherent semi-empirical simulator *SunShine* [30–32] is
24
25 used for modelling of structures with flat interfaces. Light scattering at native nano-roughness of
26
27 CIGS films can be included and modelled by scalar scattering theory [35,36]. This model enables
28
29 very fast simulations of structures comprising both, stack of thin layers presenting solar cell
30
31 (considering coherent light propagation) and thick layers (incoherent light propagation) such as
32
33 encapsulation and protection glass.
34
35
36
37

38
39 The second simulator we utilized is Comsol Multiphysics [37] where we implement a three-
40
41 dimensional model of the device. The simulator solves Maxwell equations by means of Finite
42
43 Element Method (FEM) [38]. This method enables us to model realistic three-dimensional
44
45 structures including the exact morphology of (periodically) nano-textured interfaces. However,
46
47 FEM method has practical limitations on the size of the simulation domain (micrometers) and
48
49 also considers only coherent propagation of light (thin coherent layers). To simulate the entire
50
51 vertical structure of a PV module, including the thick incoherent glass-encapsulation stack, we
52
53 make use of a previously developed method that enables the application of FEM on thick low
54
55 absorbing incoherent layers [39].
56
57
58
59
60
61
62
63
64
65

1
2
3
4 When introducing nano-textures to the substrate of the thin-film stacks, one has to consider
5
6 realistic transfer of the texture throughout the multi-layer stack. A three-dimensional model of
7
8 non-conformal layer growth [34,40] was employed together with FEM simulations to consider
9
10 the transfer of the nano-texture morphology from the rear side (substrate) to the front side of the
11
12 CIGS device. This empirical model combines two growth principles: the direct conformal growth
13
14 (i.e. growth in vertical direction) and the isotropic growth (i.e. growth in all directions). The ratio
15
16 between the two growth mechanisms is defined by a factor g in the model, ranging from 0 (fully
17
18 conformal growth) to 1 (fully isotropic growth). The values in between present linear
19
20 combinations of the two principles of growths. The model has been applied to different thin-film
21
22 materials [40] and was here calibrated for thin CIGS devices (see model calibration section).
23
24
25
26
27
28

29 Finally, for optical simulations of larger textures in the range of several μm to mm (e.g. the
30
31 texture of the light management (LM) foil), a combined wave-optics / ray-tracing simulator
32
33 CROWM was used [33]. Thin layers (e.g. cell structure) are simulated with transfer matrix
34
35 method [41] in this case, whereas full three-dimensional ray tracing is performed in micro-
36
37 textured thick incoherent layers (such as LM foil).
38
39
40
41

42 Using presented models, we can simulate wavelength-dependent reflectance and transmittance of
43
44 the entire structures, determine absorptances of individual layers, charge-carrier distributions of
45
46 generated charges and other internal quantities if needed. In all simulations we assume that lateral
47
48 dimensions of the structures are larger than vertical ones, therefore edge effects are not taken into
49
50 account.
51
52
53

54 To determine external solar cell parameters which are directly linked to optical behavior, i.e.
55
56 EQE and J_{sc} , we consider the following simplifications: ideal extraction of charge carriers from
57
58 the CIGS absorber (assuming efficient surface passivation [11], in our case with a Al_2O_3 film)
59
60
61
62
63
64
65

and neglecting the contribution of the generated carriers from the CdS layer [42] (which may affect only the short-wavelength part of EQE). Considering these assumptions, the EQE can be equalized with absorptance curve of the CIGS layer (we denote such obtained EQE as EQE_{opt}). Applying the AM1.5g solar spectrum we calculated the J_{sc} from the EQE_{opt} . For more accurate investigation of electrical properties, advanced electrical simulations are needed [43,44].

2.2 Calibration of models

Calibration of models to realistic properties of structures is important to carry out reliable simulations. In optical simulations, complex refractive indices of individual layers need to be known. In presented simulations, we use a set of realistic wavelength-dependent refractive indices, mostly obtained by ellipsometry measurements of films [42,45] or measured data published in literature [46]. Selected data are presented in Figure 1. These complex refractive indices were already used previously in experimental verification of models and show good correspondence to measured characteristics of CIGS solar cells [23].

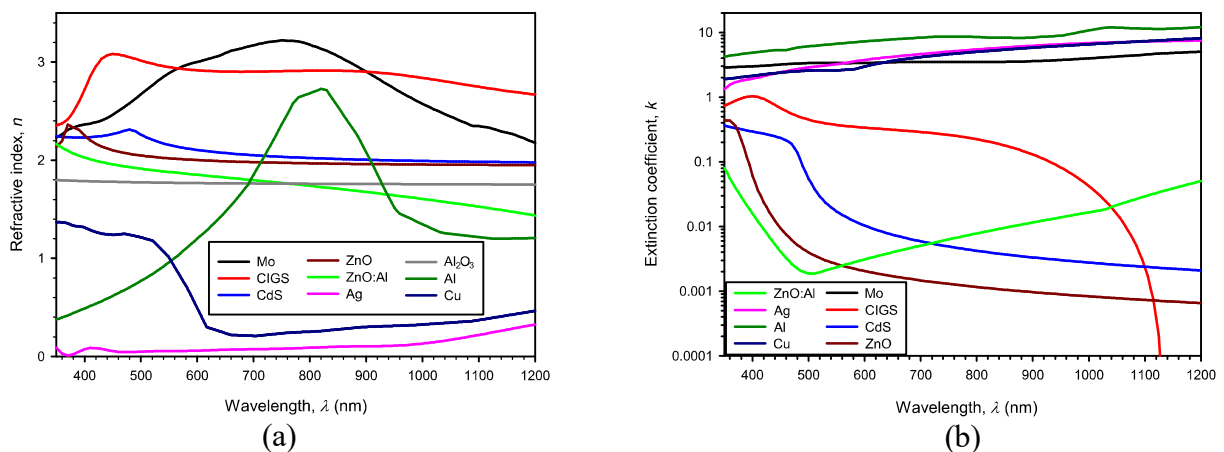


Figure 1: Refractive indices of CIGS solar cells materials: (a) real refractive index and (b) extinction coefficient.

1
2
3
4 To check layer thicknesses and to determine a suitable value of the growth parameter g for the
5
6 model of non-conformal growth, cross-sectional scanning electron microscope (SEM) images of
7
8 devices were used. To calibrate the model of layer growth (texture transfer), we varied the
9
10 empirical parameter g and compared the modeled growth with the actual growth (Figure 2).
11
12 Different samples have been analyzed. In Figure 2, images are shown for the Mo layer deposited
13
14 on randomly textured substrate (wet-etched ZnO) and for the entire thin CIGS solar cell
15
16 fabricated on the textured substrate. The most bottom interface, presenting the initial texture was
17
18 sampled and used as an input surface morphology in the model (full yellow line in Figure 2).
19
20 Overall observation is that the samples exhibit more conformal than isotropic growth. The value
21
22 of $g = 0.3$ renders good agreement between modeled and experimental cross-section data,
23
24 surprisingly, for all included layers (see dashed yellow lines in Figure 2). If thicker layers were
25
26 used, higher sensitivity to the values of g , corresponding to different layers, could be found. The
27
28 value $g = 0.3$ was used for all thin films in the structure for predictions of textures in 3-D space
29
30 (here only 2-D cross-sections are shown). The native roughness of the CIGS layer is relatively
31
32 small due to the low layer thickness and was not considered in the simulations where other
33
34 (periodic) nano-textures were included.
35
36
37
38
39
40
41
42
43
44
45
46
47
48
49
50
51
52
53
54
55
56
57
58
59
60
61
62
63
64
65

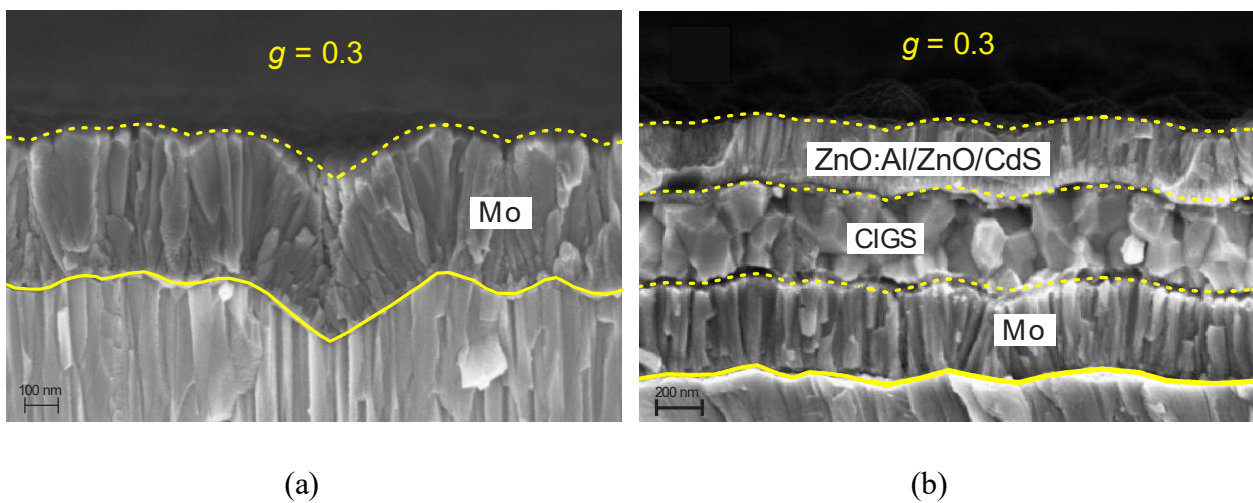


Figure 2: Cross-sectional SEM images equipped with modeled growth lines for two samples: (a) Mo layer and (b) thin CIGS cell. Bottom full yellow line in each figure present the random texture of the etched ZnO film and was used as the initial texture in the model; other (dashed) yellow lines are model predictions of layer growths.

3. Structures and textures

In our optical analysis, we considered the encapsulated solar cell structure, with front Ethyl Vinyl Acetate (EVA) encapsulation foil and protective glass, as in the PV module structure.

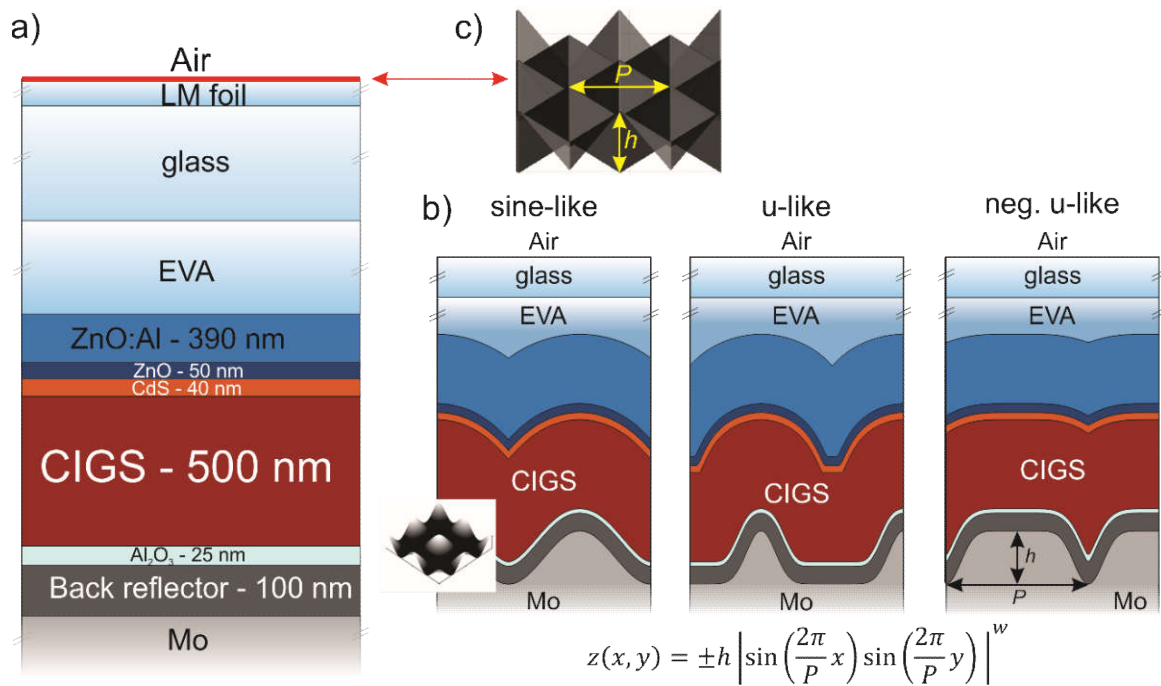


Figure 3: (a) A schematic cross-section of the thin CIGS structure with front encapsulation (PV module structure), (b) Cross-section of the structure including three types of internal textures. Non-conformal growth of thin layers is considered ($g = 0.3$) – shown for the texture sizes $P = 800$ nm, $h = 300$ nm. Textured structures from left to right: a sine-like texture (equation parameter $w = 2$), a u-like texture (wide valleys, $w = 10$) and negative u-like texture (wide hills, $w = 10$ and negative sign in equation). The equation defining the shapes of the three textures is given in the

1
2
3
4 bottom. (c) Example of a three-sided pyramid micro-texture applied to LM foil on top of the front
5
6 glass.
7
8

9
10 A schematic cross-section of the analyzed thin CIGS structure in PV module configuration is
11 presented in Figure 3 (a). In this work, we considered the thickness of the CIGS absorber $d_{\text{CIGS}} =$
12 500 nm (3.6-times thinner as in the case of the reference cell with $d_{\text{CIGS}} = 1800$ nm). Solar cell
13 layers follow in the order (from substrate to the top): a soda lime glass (SLG) substrate (not
14 shown in the schematics), an opaque Mo layer (~ 400 nm) serving as an electrical contact and a
15 back reflector (BR) in the basic case, (optional) highly reflective BR and an Al_2O_3 passivation
16 layer, CIGS absorber, CdS window layer, ZnO and ZnO:Al transparent conductive oxide contact,
17 EVA and front glass encapsulation stack and (optional) LM foil. Besides passivation, the Al_2O_3
18 layer serves also as a protective layer to prevent uncontrolled diffusion of metals used as BRs
19 into CIGS during deposition [28]. As Al_2O_3 is a non-conducting material, electrical contact can
20 be provided by an array of holes – point contacts [11–14]. Dimensions of these holes are
21 expected to be sufficiently small (e.g. ~ 100 nm and pattern pitch ~ 2 μm) and are thus not
22 considered in the present optical analysis. In case of direct evaporation of CIGS on Mo, we
23 assumed in the optical simulations a formation of MoSe_2 interfacial layer [47], decreasing the
24 reflectance of the Mo contact by ~ 20 -25 % [48]. In simulations, EVA, glass and LM foil are
25 considered as a single layer, assuming a sufficient matching in refractive indices of these layers.
26 Selected simulations with de-coupled encapsulation and LM foil stack revealed no changes in the
27 trends observed for the joined stack.
28
29
30
31
32
33
34
35
36
37
38
39
40
41
42
43
44
45
46
47
48
49
50
51
52
53

54
55 Comparison of optical behavior between the solar cell and such PV module structure was carried
56 out by optical simulations in [23]. In short, front encapsulation improves light in-coupling in the
57 solar cell if sufficiently low absorbing encapsulation and protective glass are used. In PV module
58
59
60
61
62
63
64
65

1
2
3
4 structure, the front cell-level ZnO:Al/air interface becomes a series of air/glass, glass/EVA, and
5
6 EVA/ZnO:Al interfaces, which combined have much lower reflectance than single air/ZnO:Al
7
8 interface in the basic solar cell structure. Therefore, the antireflection coating on top of ZnO:Al is
9
10 not needed in PV module configuration. The $\sim 4\%$ reflectance at front glass/air interface
11
12 predominates in this case.
13
14

15
16
17 In this paper, we study optical improvements related to three concepts: (i) introduction of highly
18
19 reflective BRs, (ii) internal nano-textures (in combinations with highly reflective BRs) and (iii)
20
21 external micro-textures realized by means of an attached LM foil. The positions of the BR and
22
23 LM foil are marked in Figure 3 (a), whereas examples of introduced internal and the external LM
24
25 textures are presented in Figure 3 (b) and (c), respectively.
26
27
28

29
30 We selected three shapes of internal nano-textures, which we introduced to the rear side of the
31
32 device (Figure 3(b)): a sine-like, u-like and negative u-like nano-texture. The investigated
33
34 textures are periodic and two-dimensional (as indicated by the insert for the sine-like texture).
35
36 The morphology of the textures is mathematically described by using the formula depicted in
37
38 Figure 3, where by changing the factor w and the positive/negative sign in equation, we can
39
40 define the textures. Applying $w = 2$ and positive sign, we obtain the sine-like, with $w = 10$ and
41
42 positive sign the u-like and with $w = 10$ and negative sign the negative u-like texture. Practically,
43
44 different kinds of textures can be fabricated by e.g. wet or dry etching techniques of the SLG
45
46 substrate, or using high- temperature resistant lacquer on the SLG, structured by UV nanoimprint
47
48 lithography [49,50]. Besides the three different shapes of the internal textures, lateral (period, P)
49
50 and vertical (height, h) sizes of the textures were varied in optical simulations. While the role of
51
52 the highly reflective BR is to reflect the transmitted (long-wavelength) light back to the thin
53
54 CIGS absorber, the purpose of the textures is to scatter (nano-textures) or refract (micro-textures)
55
56
57
58
59
60
61
62
63
64
65

1
2
3
4 light, thus to change the angle of propagation and increase optical path and light trapping inside
5
6 the cell (especially reflections from front interfaces back to CIGS due to higher incident angles
7
8 may play an important role) [51]. Additionally, light in-coupling properties can be improved in
9
10 case of textures present at the front side of the device.
11
12

13
14 The introduced internal nano-textures are transferred through thin layers to the front side of the
15
16 thin-film stack, which is described in the simulated structure by the calibrated model of non-
17
18 conformal layer growth. Indications on the interface morphology changes can be observed in
19
20 Figure 3 (b) for all three types of the nano-textures for selected $P = 800$ nm and $h = 300$ nm.
21
22 Different P and h combinations of each type of nano-textures were included in the analysis. In
23
24 simulations, the initial internal textures were introduced on top surface of the Mo layer.
25
26
27
28

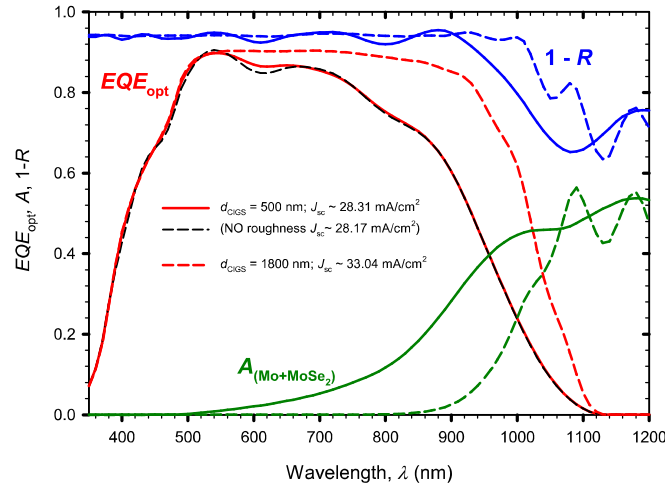
29
30 For the external textures, we selected a micro-texture with the shape of three-sided pyramid,
31
32 applied (e.g. via embossing) to the LM foil (made of lacquer or PDMS material). Such kind of
33
34 textures showed good results in improving optical performances of other types of thin-film solar
35
36 cells, such as thin-film silicon solar cells as well as organic and perovskite solar cells [51–54]. A
37
38 basic version of such a texture with 90° angle between the planes is known as a corner cube
39
40 texture, with the aspect ratio $AR = h / P = 0.71$. Here different aspect ratios of the texture were
41
42 simulated to find optimal shape of such kind of the texture for our investigated device. Due to
43
44 larger dimensions of this LM foil texture ($P = 9 \mu\text{m}$), ray optics in combination with thin-film
45
46 optics need to be used (CROWM simulator).
47
48
49
50
51
52
53
54
55

56 **4. Results and discussion**

57 **4.1 Optical simulations of initial CIGS structure**

58
59
60
61
62
63
64
65

1
2
3
4 Firstly, we simulated the initial CIGS (PV module) structure and identified optical losses. In this
5
6 structure, we consider flat Mo back contact (no additional BR used). The effect of the front
7
8 random native roughness of thin CIGS (root-mean-square roughness measured to be $\sigma_{\text{rms}} = 40$
9
10 nm) was also checked. 1-D optical simulator SunShine was used in these simulations. Selected
11
12 simulation results are plotted in Figure 4. $EQE_{\text{opt}} (A_{\text{CIGS}})$. The total reflection R at the top surface
13
14 of the PV module (presented as $1-R$) and absorption losses in the back contact are shown for the
15
16 thin CIGS structure ($d_{\text{CIGS}} = 500$ nm) and compared to the results obtained for the reference
17
18 structure ($d_{\text{CIGS}} = 1800$ nm). Thin CIGS structures were simulated with and without considering
19
20 the native CIGS roughness, whereas the thick CIGS structure was simulated only with the native
21
22 roughness of thicker CIGS film ($\sigma_{\text{rms}} = 57$ nm [48]).
23
24
25
26
27
28



29
30
31
32
33
34
35
36
37
38
39
40
41
42
43
44
45
46
47
48
49
50
51
52
53
54
55
56
57
58
59
60
61
62
63
64
65
Figure 4: $EQE_{\text{opt}} (A_{\text{CIGS}})$, reflection losses ($1-R$) and absorption losses in back Mo-based contact of a standard thick (1800 nm) and thin (500 nm) CIGS module. Added is an EQE_{opt} for thin absorber, without considering the native roughness of CIGS layer.

53
54
55
56
57
58
59
60
61
62
63
64
65
We can observe that the structure with 500 nm thick CIGS absorber exhibits a reduced EQE_{opt} already from $\lambda = 550$ nm onwards, compared to the structure with 1800 nm thick absorber. This decrease is also reflected in J_{sc} , where the value of 33.04 mA/cm^2 is obtained for the structure

1
2
3
4 with thick absorber and 28.31 mA/cm² for the structure with thin absorber ($\Delta J_{sc} = 4.73$ mA/cm²,
5
6 i.e. 14.3 %).
7
8

9
10 Highly distinctive is also increased absorptance in the back contact (Mo+MoSe₂) for the thin
11
12 CIGS structure in the wavelength region $500 \text{ nm} < \lambda < 1000 \text{ nm}$ as more light is transmitted to
13
14 the back contact. Comparison of the $1-R$ curves indicates a decrease (thus increase in R) at 900
15
16 nm $< \lambda < 1100 \text{ nm}$ for the structure with thin absorber, indicating less overall absorption in the
17
18 structure in this wavelength region. Observations related to $A_{(\text{Mo}+\text{MoSe}_2)}$ indicate that in the thin
19
20 structure one should reduce optical losses in the rear contact – i.e. introduction of a highly
21
22 reflective BR is a need.
23
24
25

26
27 Additionally, in Figure 4, we added EQE_{opt} for the thin structure without considering the native
28
29 CIGS roughness, showing only small differences to the EQE_{opt} (observable in the wavelength
30
31 region $500 < \lambda < 700 \text{ nm}$) and J_{sc} of the structure where the random native roughness was
32
33 considered. Due to relatively small differences, this native texture was not considered in further
34
35 simulations of thin devices.
36
37
38
39
40
41

42 43 **4.2 Optical improvements related to highly reflective back contacts**

44
45 Different metal-based BRs were employed in simulations. Introduction of alternative metal BRs
46
47 involves also a thin passivation layer of Al₂O₃ material [11–14], serving as a passivation and as
48
49 well as a metal diffusion barrier [28]. The results are presented for the following BRs: Cu, Al, Ag
50
51 and Mo as a reference (this time also passivated with Al₂O₃ as all the others).
52
53
54
55

56
57 We firstly carried out simulations on flat standalone BR samples and compared the simulated
58
59 reflectance curves to the measured ones. In Figure 5 (a), measured and simulated results are
60
61
62
63
64
65

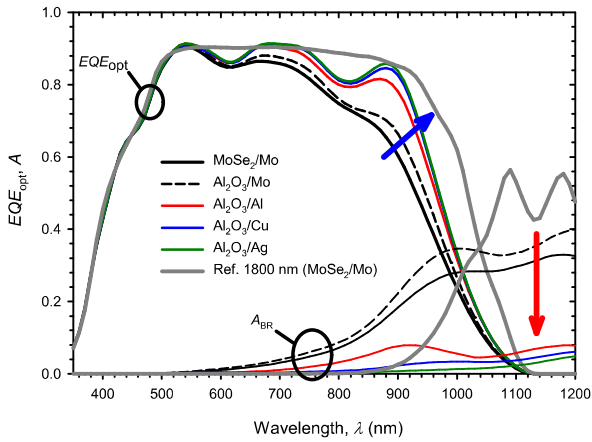
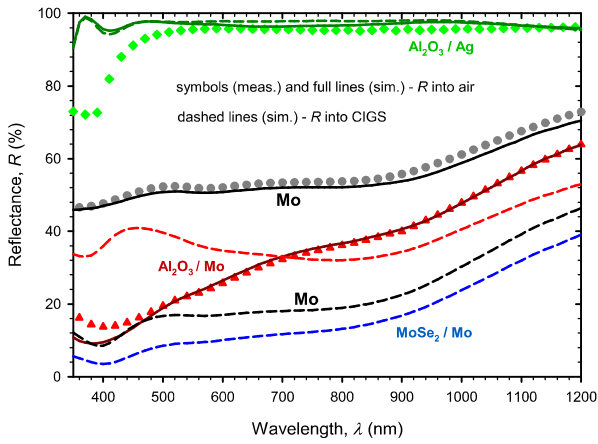
1
2
3
4 shown for the Mo, Al₂O₃/Mo and Al₂O₃/Ag reflectors fabricated on SLG. Please note that the
5
6 order of named layers in the stacks (here and later on) corresponds to the direction of light
7
8 impinging and not to the layer deposition sequence. All samples had an opaque layer of Mo
9 (~400 nm) on SLG. In Al₂O₃/Mo sample, the thickness of Al₂O₃ was 45 nm while the layer
10
11 thicknesses in the Al₂O₃/Ag sample were 90 nm for Al₂O₃ and 100 nm for the Ag layer. First, we
12
13 analyze the reflectance as measured/simulated in air (symbols and full lines). Good agreement is
14
15 obtained between simulated and measured results, confirming the suitability of the complex
16
17 refractive indices of layers used in simulations. The reflectance of bare Mo contact facing air is >
18
19 50 % at $\lambda > 550$ nm and decreases when adding thin Al₂O₃ layer on top of it. As we will show
20
21 later, this is not present if simulating the reflectance into the CIGS absorber. In case of air as
22
23 incident medium, thin Al₂O₃ acts as an antireflective rather than reflective coating, due to gradual
24
25 refractive index transition from air to Mo in this case. Measurements and simulations of
26
27 Al₂O₃/Ag reflector show high (long-wavelength) reflection (> 95 % in air).
28
29
30
31
32
33
34
35

36 To approach the optical situation in the CIGS structure, we simulated the reflectance of the BRs
37
38 into the CIGS absorber (dashed lines in Figure 5). The reflectance of Mo into CIGS appears to be
39
40 quite low, with values below 50 % over entire wavelength range and below 20 % for $\lambda < 850$ nm.
41
42 In practical cases a MoSe₂ layer between Mo and CIGS is formed during CIGS deposition which
43
44 reduces the reflection into CIGS by an additional 20-25%. Generally, reflection of a Mo (also
45
46 MoSe₂/Mo) BR into CIGS is much lower than into air due to changed Fresnel coefficients,
47
48 considering refractive indices of the adjacent layers. When adding an Al₂O₃ layer to Mo, we
49
50 expect the formation of MoSe₂ layer is prevented, which results in higher R over the entire
51
52 spectral range. An interesting observation is also, that adding an Al₂O₃ layer increases the
53
54 reflection into CIGS, for both Mo and Ag back reflectors, while the opposite trend (reduction of
55
56
57
58
59
60
61
62
63
64
65

1
2
3
4 R) was observed for reflection into air. Finally, reflection of $\text{Al}_2\text{O}_3/\text{Ag}$ into CIGS is high
5
6 compared to reflection into air.
7
8

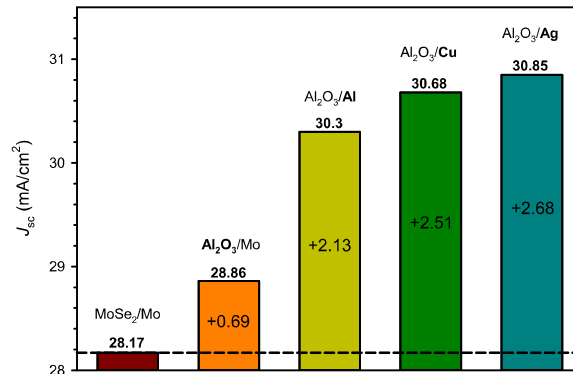
9
10 The BRs were included in simulations of the complete PV module structure. EQE_{opt} and optical
11 losses in the BRs (A_{BR}) are presented in Figure 5(b), while the corresponding J_{sc} values are
12 plotted in Figure 5(c). By using the alternative BRs, we can observe an increase in EQE_{opt} for
13 wavelengths over 550 nm. Small increase can already be observed for Mo with Al_2O_3 layer,
14 while much larger increase is observable for other highly reflective metal BRs (see blue arrow in
15 Figure 5(b)). As an origin of increased EQE_{opt} we can also notice highly reduced parasitic
16 absorption in BR (see red arrow in Figure 5(b)).
17
18
19
20
21
22
23
24
25
26

27 The trend observed in EQE_{opt} in Figure 5(b) is reflected also in J_{sc} values presented in Figure
28 5(c). Using a standard MoSe_2/Mo BR resulted in a relatively low $J_{\text{sc}} = 28.17 \text{ mA/cm}^2$ as indicated
29 already in Figure 4 for the flat device. Adding Al_2O_3 to Mo (and excluding MoSe_2) already
30 increases the J_{sc} to 28.86 mA/cm^2 (+ 2.4 %). Expectedly, for the Ag-based BR the highest $J_{\text{sc}} =$
31 30.85 mA/cm^2 is obtained, which is 9.5 % improvement towards starting MoSe_2/Mo BR.
32
33
34
35
36
37
38
39
40
41
42
43
44
45
46
47
48
49
50
51
52
53
54
55
56
57
58
59
60
61
62
63
64
65



(a)

(b)



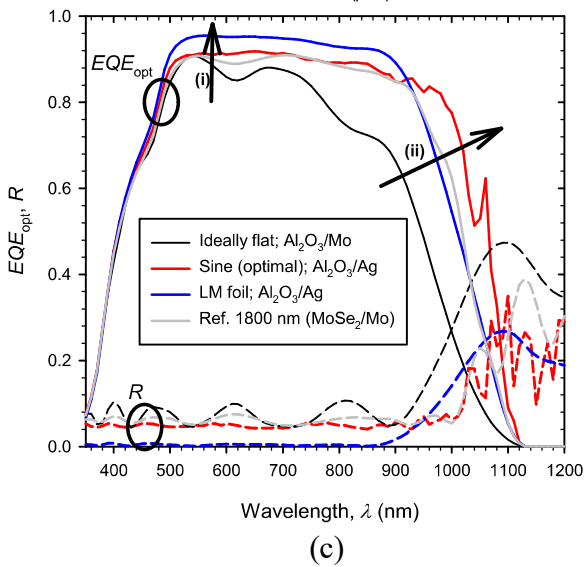
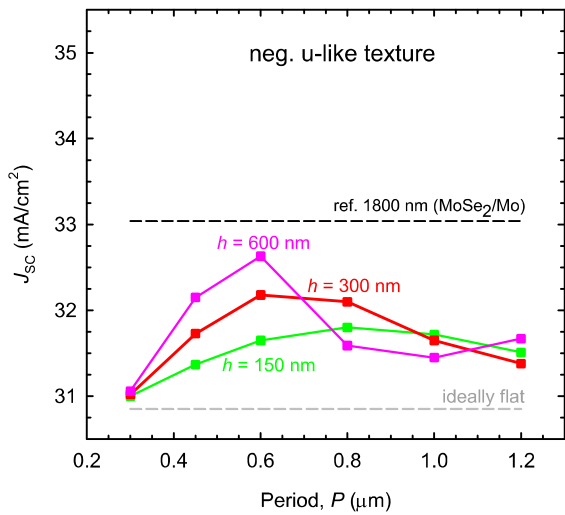
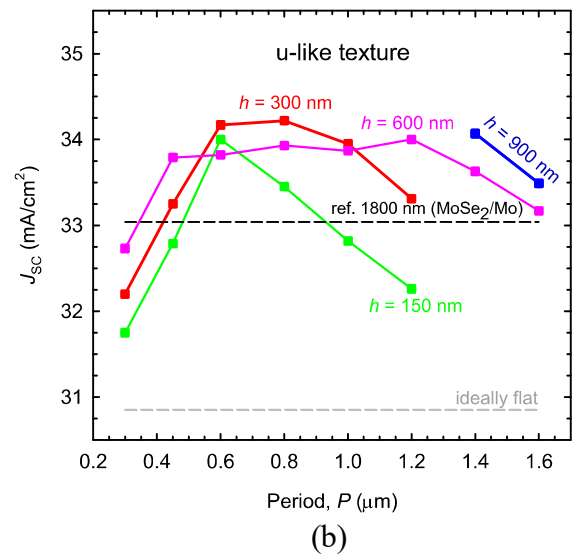
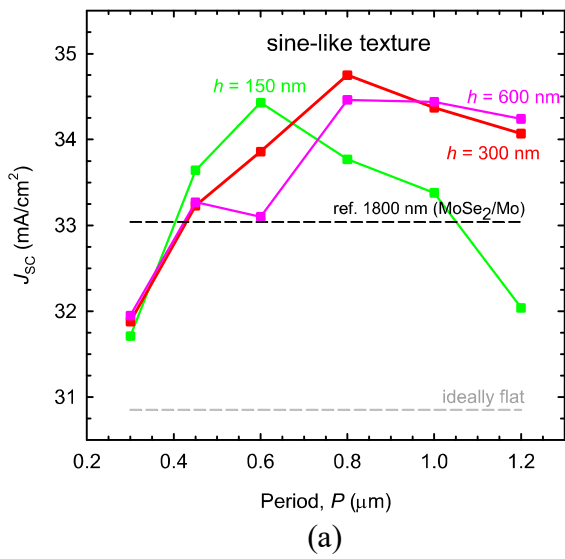
(c)

Figure 5: (a) Reflectance measurements and simulations of different BRs. (b) Simulated EQE_{opt} (A_{CIGS}) and absorption losses in BRs for the PV module structure with $d_{CIGS} = 500$ nm (the structure with $d_{CIGS} = 1800$ nm and MoSe₂/Mo BR is added as a reference) (c) comparison of simulated J_{sc} for different BRs and $d_{CIGS} = 500$ nm. All structures have flat interfaces in this case.

1
2
3
4 These results show that the highest J_{sc} achieved by using the Ag BR still exhibit lower J_{sc} than
5
6 the one of the thick CIGS cell (33.04 mA/cm²). Thus, additional light management is necessary
7
8 to reach and possibly surpass the J_{sc} of the thick device.
9

10 11 12 13 14 **4.3 Optical effects of internal textures**

15
16
17 To improve the J_{sc} of the thin CIGS devices further, we investigate the potential of internal nano-
18
19 textures introduced to the rear side of the device (textured BRs). Nano-textures in general
20
21 promote light scattering and antireflection at front interfaces, which can increase light in-coupling
22
23 and trapping inside thin CIGS absorber. Using 3-D FEM simulations with Comsol, we studied
24
25 the role of three different periodic textures, as schematically presented in Figure 3 (c). Besides
26
27 different shapes of the textures, lateral and vertical dimensions (P and h) were varied in
28
29 simulations. It has to be noted that textures have been optimized here from the optical point of
30
31 view, while possible effects on electrical properties of layers and interfaces have not been
32
33 investigated. Therefore, we show in Figure 6 the results of J_{sc} for a broader span of texture
34
35 dimensions P and h to enable to consider possible trade-offs with respect to electrical properties
36
37 if affected (not in the scope of this paper).
38
39
40
41
42
43
44
45
46
47
48
49
50
51
52
53
54
55
56
57
58
59
60
61
62
63
64
65



1
2
3
4 Figure 6: Simulated J_{sc} dependence on period (P) and height (h) of different textures for the PV
5 module structure with $d_{CIGS} = 500$ nm and Al_2O_3/Ag BR: (a) sine-like texture, (b) u-like texture ,
6
7
8 (c) negative u-like texture and (d) EQE_{opt} and reflectance (R) comparison for the structures with
9 optimal sizes of sine-like textures ($P = 800$ nm, $h = 300$ nm) and for the structure with optimized
10 LM foil for Al_2O_3/Ag and Al_2O_3/Mo BR; the arrow (i) indicates the improvements related to light
11 in-coupling (with the LM foil), whereas the arrow (ii) shows the effect mostly related to
12 improved light trapping.
13
14
15
16
17
18
19
20
21
22
23
24

25 In Figure 6 (a-c), we show simulated J_{sc} results corresponding to the three internal nano-texture
26 types (sine-, u- and negative u-like) for the PV module structure with Al_2O_3/Ag BR and $d_{CIGS} =$
27 500 nm. Exceptions are the top reference lines which correspond to the J_{sc} of the PV module with
28 $d_{CIGS} = 1800$ nm and $MoSe_2/Mo$ BR. The bottom reference lines represent an ideally flat PV
29 module with $d_{CIGS} = 500$ nm and Al_2O_3/Ag BR. Later on, we will show that the choice of a highly
30 reflective BR is crucial to get high J_{sc} improvements related to the internal textures. For the case
31 of Al_2O_3/Ag BR effects of variations in P and h are shown for all three texture types in Figure 6
32 (a-c).
33
34
35
36
37
38
39
40
41
42
43
44

45 The results show that the highest gain is obtained for sine shaped texture, reaching the maximum
46 J_{sc} of 34.75 mA/cm² at $P = 800$ nm and $h = 300$ nm. This value exceeds the J_{sc} of 1800 nm thick
47 (33.04 mA/cm²) reference CIGS PV-module. It has to be noted that P s and h s have not been
48 optimized further in smaller steps as presented in the plots. Comparing the EQE_{opt} that
49 corresponds to the flat CIGS structure ($d_{CIGS} = 500$ nm) and the one corresponding to the sine-
50 like texture in Figure 6 (d) we can observe that the main gain is obtained due to the enhanced
51 CIGS absorption in the long-wavelength region. This is mainly due to light scattering at textured
52
53
54
55
56
57
58
59
60
61
62
63
64
65

1
2
3
4 interfaces and consequently light trapping in the structure. A spike, that can be noticed in EQE_{opt}
5
6 at longer wavelengths, is a pronounced interference peak caused by resonance behavior of the
7
8 specific combination of P , h , and layer thicknesses. Additionally, we also present total reflectance
9
10 for flat and nano-textured BRs. Due to transfer of texture to the front of the cell, some
11
12 antireflection effect occurs, resulting in reduced short-wavelength region reflection as well,
13
14 whereas in the long-wavelength region, the total reflectance is lower due to better trapping of
15
16 light inside the device.
17
18
19
20
21

22 For selected P and h combinations (optima from Figure 6 (a-c)) we carried out a more detailed
23
24 analysis of optical effects. In particular we de-coupled the effects of light trapping and the
25
26 antireflection effects, both related to the introduced periodic nano-textures. Additional
27
28 simulations of partial device structures, where antireflection effect itself (improved in-coupling
29
30 into the CIGS absorber layer) was evaluated separately by comparing the transmission of light
31
32 into the absorber with or without the textures transferred to the front side of the device. The
33
34 remaining gain we assigned to the light trapping. In order to indicate the crucial role of highly
35
36 reflective BR in combination with the introduced nano-textures, we also included in this analysis
37
38 MoSe₂/Mo and Al₂O₃/Mo reflectors.
39
40
41
42
43

44 The results of the analysis are presented on the level of J_{sc} in Figure 7. Four groups of bars
45
46 correspond to the three different internal textures and the fourth one to the structure with LM foil
47
48 (and flat internal interfaces), which will be discussed in section 4.4. Each group of bars contains
49
50 simulated J_{sc} results corresponding to the mentioned three BRs (MoSe₂/Mo, Al₂O₃/Mo and
51
52 Al₂O₃/Ag). The shaded parts of bars indicate the J_{sc} level of the ideally flat structures and differ
53
54 only with the BR type (the same pattern of J_{sc} level recognized in all four groups of bars). A
55
56 reference line corresponding to the structure with $d_{CIGS} = 1800$ nm and MoSe₂/Mo BR is added.
57
58
59
60
61
62
63
64
65

First we can observe that the gains related to different textures are much lower for the $\text{Al}_2\text{O}_3/\text{Mo}$ and especially MoSe_2/Mo reflectors, compared to the $\text{Al}_2\text{O}_3/\text{Ag}$ one. This confirms that highly reflective BR has to be used in combinations with the introduced nano-textures to fully explore their potential. If high reflectance is not assured, optical losses are increased significantly in the BRs, due to introduced textures, limiting the absorptance in thin CIGS severely.

The de-coupling of the antireflection and light trapping contribution is shown only for the case of the structures with $\text{Al}_2\text{O}_3/\text{Ag}$ BR. The total J_{sc} values correspond the values of structures with optimal P and h combinations from Figure 6 (a-c). The de-coupling shows that in case of internal textures the light trapping effects predominates the antireflection ones (e.g. in the case of sine-like texture for more than 5.6-times).

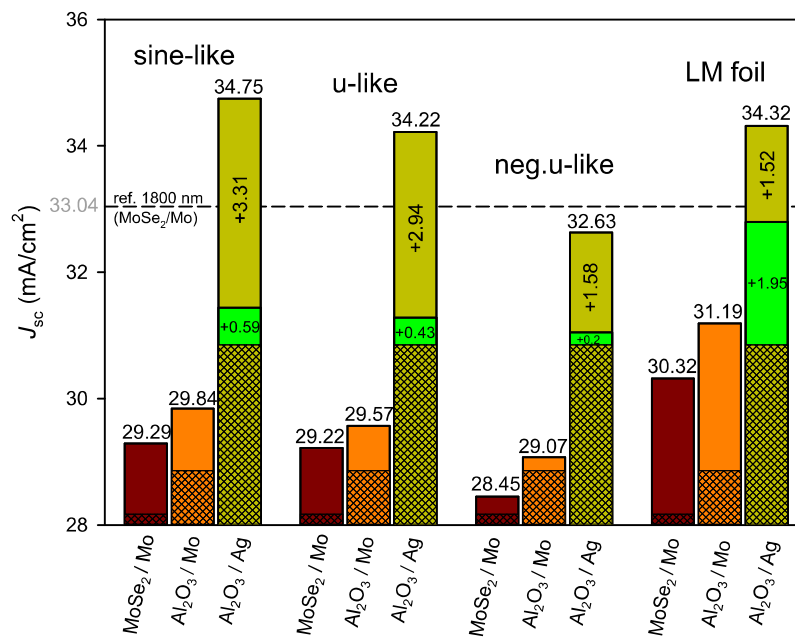
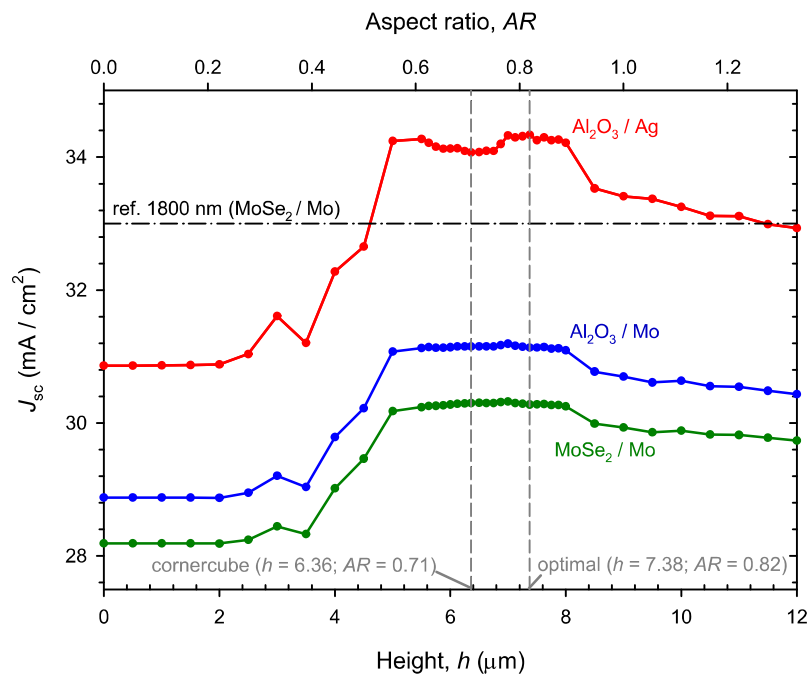


Figure 7: Comparison of simulated J_{sc} for selected internal textures and external LM foil for three different BRs. The meshed parts represent J_{sc} level of flat devices. For textures on $\text{Al}_2\text{O}_3/\text{Ag}$ BR light green parts of the bars represent the contributions of the antireflection effect (increased light transmission into CIGS absorber) due to textures and the rest is due to light scattering & trapping.

4.4 Improvements related to external textures

If external textures are applied, electrical properties of the layers in the solar cell structure remain intact: the internal interfaces remain flat and the external texture is applied after solar cell fabrication via LM foil on the top surface of the front glass in the analyzed concept. Textures with feature sizes of several micrometers, namely $P = 9 \mu\text{m}$ and different values of h (0-12 μm), are considered in our analysis and CROWM simulator is used for simulations. Example for the applied three-sided pyramid external texture was shown in Figure 3 (b). Keeping the P constant, the h and consequently the AR of the texture was varied to optimize light management behavior of the LM foil for the thin CIGS device. In Figure 8 we present J_{sc} dependence on the AR (and h) of the presented LM foil textures for different BRs, the standard MoSe_2/Mo , $\text{Al}_2\text{O}_3/\text{Mo}$ and $\text{Al}_2\text{O}_3/\text{Ag}$. The thickness of the absorber was again $d_{\text{CIGS}} = 500 \text{ nm}$, except for the thick reference cell. Results show that similarly as with textured BR, highest J_{sc} are observable for $\text{Al}_2\text{O}_3/\text{Ag}$ BR for all AR s.



1
2
3
4 Figure 8: Simulated J_{sc} dependence on the aspect ratio (h / P) of LM three-sided pyramid texture
5
6 for different BRs.
7
8

9
10 Sweep over different AR s reveals that the highest $J_{sc} = 34.33 \text{ mA/cm}^2$ is found at AR around 0.82
11
12 ($h = 7.375 \text{ um}$), however distinct broader plateaus are observed in the region of increased J_{sc} . The
13
14 cornercube texture ($AR = 0.71$), lies on the plateaus of increased J_{sc} . With additional optimization
15
16 of the the LM foil texture, by changing the AR from 0.71 to $AR \sim 0.82$, slightly higher J_{sc} can be
17
18 achieved ($\sim 0.7 \%$).
19
20
21

22
23 In case of external micro-textures, the geometrical optics is considered for locally reflected and
24
25 transmitted light. Due to re-direction of reflected and transmitted light and due to the corrugations
26
27 of the surface, the rays may experience multiple entering events as well as redirection of
28
29 propagation inside the structure. Moreover, the texture importantly also affects the level of
30
31 trapping of backward propagating rays, which have not been fully absorbed in previous passes
32
33 throughout the structure. Detailed analysis of optical situation revealed that by increasing the AR
34
35 of the texture from 0 and up, first the antireflection effect (multiple entering events) is gradually
36
37 allowing more light into the structure. Increasing the AR further, due to favorable angles of the
38
39 three-sided texture, more upward light gets back reflected (trapped), resulting in an increased
40
41 absorption. AR s between 0.55 and 0.85 are favorable for light trapping, resulting in increased J_{sc} ,
42
43 as observed in Figure 8 for all BRs. By increasing the AR further, angles in the texture become
44
45 too high to enable efficient light trapping, letting more reflected light escape into air, reducing the
46
47 J_{sc} . Simulations also indicated that the extension of a single light path through the absorber due to
48
49 refraction is almost negligible no matter the AR . A more detailed explanation of the presented
50
51 effects, which are expressed also in other PV structures, can be found in [51].
52
53
54
55
56
57
58
59
60
61
62
63
64
65

1
2
3
4 Simulation results reveal, that the structure with the cornercube texture and $\text{Al}_2\text{O}_3/\text{Ag}$ BR
5
6 increases the J_{sc} up to 34.23 mA/cm^2 , which is already more than the reference thick CIGS device
7
8 and close to the values obtained with textured BRs, as shown in Figure 7. For the structures with
9
10 MoSe_2/Mo and $\text{Al}_2\text{O}_3/\text{Mo}$ BR, J_{sc} is increased by adding the LM foil compared to the structure
11
12 without the LM foil, but values remain below the 1800 nm thick CIGS structure. However, as can
13
14 be seen in Figure 7, weakly reflecting BRs behave better in combination with the LM foil as with
15
16 internal textures. Moreover, the contribution of antireflection effect to the gain in J_{sc} is here much
17
18 larger than in case of internal textures.
19
20
21
22
23
24
25
26

27
28 EQE_{opt} and R of the structure with the LM foil (see Figure 6 (d)) indicate that LM foil improves
29
30 the performance (higher EQE_{opt} and lower R) over entire wavelength range as a consequence of
31
32 broadband antireflection behavior and trapping effect for optimized AR , although the trapping of
33
34 long-wavelength light is smaller as in case of optimized internal textures.
35
36
37
38
39
40

41 **5. Conclusions**

42
43
44 Using calibrated optical modelling, we first indicated optical losses in thin CIGS devices with
45
46 500 nm thick CIGS absorber. Comparison of simulated EQE_{opt} for the PV module structure with
47
48 a thick ($d_{\text{CIGS}} = 1800 \text{ nm}$) and thin ($d_{\text{CIGS}} = 500 \text{ nm}$) absorber reveals highly reduced absorption
49
50 in case of the thin CIGS layer above $\lambda = 550 \text{ nm}$ and enhanced optical losses at the poorly
51
52 reflecting Mo back contact. To increase the EQE and J_{sc} we first analyze the potential
53
54 improvements related to the introduction of highly reflective metals in the role of BRs. Among
55
56 simulated $\text{Al}_2\text{O}_3/\text{Mo}$, $\text{Al}_2\text{O}_3/\text{Al}$, $\text{Al}_2\text{O}_3/\text{Cu}$ and $\text{Al}_2\text{O}_3/\text{Ag}$ BRs, the Ag based reflector showed
57
58
59
60
61
62
63
64
65

1
2
3
4 highest potential, with more than 9.5 % improvement towards a standard MoSe₂/Mo back
5
6 reflector. According to simulations the usage of a highly reflective Al₂O₃/Ag back reflector,
7
8 effectively reduces the absorption losses at the back contact, but even for the best case of Ag BR,
9
10 the improved J_{sc} does not match the J_{sc} of the structure with thick CIGS absorber.
11
12

13
14 To further improve J_{sc} of the thin device and to approach optical performance of the thick one,
15
16 the potential gain related to internal nano-texturing was studied by means of 3-D optical
17
18 simulations. Three different internal textures, including realistic layer growth and highly
19
20 reflective Al₂O₃/Ag BR, were evaluated. All textures showed improvement in J_{sc} relative to flat
21
22 structures, by increasing the absorption in CIGS at the long wavelengths, mainly due to light
23
24 scattering and trapping. Highest improvements were achieved with a sine texture ($P = 800$ nm, h
25
26 = 300 nm) peaking at 34.75 mA/cm², which surpasses the J_{sc} of the structure with thick CIGS
27
28 absorber (+1.71 mA/cm²).
29
30
31

32
33 Additionally, to avoid possible influence of texturing on electrical performance, textures were
34
35 applied on the external interface (air / front sheet glass) by a LM foil, comprising a three sided
36
37 pyramid texture. Using LM foil, all other interfaces were kept flat. External texture optimization
38
39 was carried out and a high J_{sc} of 34.33 mA/cm² was predicted, surpassing the J_{sc} of thick standard
40
41 module for +1.29 mA/cm². For the simulated external textures, the increased J_{sc} , was due to
42
43 antireflection and light scattering & trapping in similar ratios.
44
45
46
47
48

49
50 The usage of textures (internal and external) was also simulated with standard Mo BR. For
51
52 internal textures only marginal improvements to the J_{sc} were observed, much lower than with
53
54 usage of alternative highly reflective back reflector (flat or with textures). For external textures
55
56 with standard Mo BR, higher improvements were obtained, but still J_{sc} does not reach the one of
57
58 thick absorber. Much larger improvements in J_{sc} for thin CIGS absorber can be achieved using an
59
60
61
62
63
64
65

1
2
3
4 alternative highly reflective BR, compared to introducing textures in combination with a standard
5
6 Mo BR. Hence, to compensate for the J_{sc} drop of thin CIGS, a combination of highly reflective
7
8 back contact and introduction of textures (internal or external) is needed.
9

10 11 12 13 14 15 **Acknowledgement**

16
17
18 The authors acknowledge the financial support of the H2020 project ARCIGS-M (GA No. 720887 -
19
20 H2020 NMBP-2016-2017).
21
22

23 24 25 **6.) References**

- 26
27
28 [1] Solar Frontier hits 23.35% efficiency with thin-film cell, Renewablesnow.Com. (n.d.).
29 /news/solar-frontier-hits-2335-efficiency-with-thin-film-cell-639947/ (accessed February 7,
30 2019).
31
32 [2] H. Sugimoto, High efficiency and large volume production of CIS-based modules, in: 2014
33 IEEE 40th Photovolt. Spec. Conf. PVSC, 2014: pp. 2767–2770.
34 doi:10.1109/PVSC.2014.6925503.
35
36 [3] M. Powalla, S. Paetel, E. Ahlswede, R. Wuerz, C.D. Wessendorf, T. Magorian Friedlmeier,
37 Thin-film solar cells exceeding 22% solar cell efficiency: An overview on CdTe-,
38 Cu(In,Ga)Se₂-, and perovskite-based materials, Appl. Phys. Rev. 5 (2018) 041602.
39 doi:10.1063/1.5061809.
40
41 [4] H.U. Sverdrup, K.V. Ragnarsdottir, D. Koca, An assessment of metal supply sustainability
42 as an input to policy: security of supply extraction rates, stocks-in-use, recycling, and risk
43 of scarcity, J. Clean. Prod. 140 (2017) 359–372. doi:10.1016/j.jclepro.2015.06.085.
44
45 [5] British Geological Survey, Risk list 2015, (n.d.).
46 http://www.bgs.ac.uk/mineralsuk/statistics/riskList.html.
47
48 [6] J. Posada, M. Jubault, N. Naghavi, Ultra-thin Cu(In,Ga)Se₂ solar cells prepared by an
49 alternative hybrid co-sputtering/evaporation process, Thin Solid Films. 633 (2017) 66–70.
50 doi:10.1016/j.tsf.2016.08.015.
51
52 [7] N. Naghavi, F. Mollica, J. Goffard, J. Posada, A. Duchatelet, M. Jubault, F. Donsanti, A.
53 Cattoni, S. Collin, P.P. Grand, J.J. Greffet, D. Lincot, Ultrathin Cu(In,Ga)Se₂ based solar
54 cells, Thin Solid Films. 633 (2017) 55–60. doi:10.1016/j.tsf.2016.11.029.
55
56 [8] A. Loubat, C. Eypert, F. Mollica, M. Bouttemy, N. Naghavi, D. Lincot, A. Etcheberry,
57 Optical properties of ultrathin CIGS films studied by spectroscopic ellipsometry assisted by
58 chemical engineering, Appl. Surf. Sci. 421 (2017) 643–650.
59 doi:10.1016/j.apsusc.2016.10.037.
60
61 [9] F. Mollica, M. Jubault, F. Donsanti, A. Loubat, M. Bouttemy, A. Etcheberry, N. Naghavi,
62 Light absorption enhancement in ultra-thin Cu(In,Ga)Se₂ solar cells by substituting the
63
64
65

back-contact with a transparent conducting oxide based reflector, *Thin Solid Films*. 633 (2017) 202–207. doi:10.1016/j.tsf.2016.10.006.

- [10] L.M. Mansfield, A. Kanevce, S.P. Harvey, K. Bowers, C. Beall, S. Glynn, I.L. Repins, Efficiency increased to 15.2% for ultra-thin Cu(In,Ga)Se₂ solar cells, *Prog. Photovolt. Res. Appl.* 26 (2018) 949–954. doi:10.1002/pip.3033.
- [11] P.M.P. Salomé, B. Vermang, R. Ribeiro- Andrade, J.P. Teixeira, J.M.V. Cunha, M.J. Mendes, S. Haque, J. Borme, H. Águas, E. Fortunato, R. Martins, J.C. González, J.P. Leitão, P.A. Fernandes, M. Edoff, S. Sadewasser, Passivation of Interfaces in Thin Film Solar Cells: Understanding the Effects of a Nanostructured Rear Point Contact Layer, *Adv. Mater. Interfaces*. 5 (2018) 1701101. doi:10.1002/admi.201701101.
- [12] B. Vermang, J.T. Wätjen, C. Frisk, V. Fjällström, F. Rostvall, M. Edoff, P. Salomé, J. Borme, N. Nicoara, S. Sadewasser, Introduction of Si PERC Rear Contacting Design to Boost Efficiency of Cu(In,Ga)Se₂ Solar Cells, *IEEE J. Photovolt.* 4 (2014) 1644–1649. doi:10.1109/JPHOTOV.2014.2350696.
- [13] S. Suresh, J. de Wild, T. Kohl, D.G. Buldu, G. Brammertz, M. Meuris, J. Poortmans, O. Isabella, M. Zeman, B. Vermang, A study to improve light confinement and rear-surface passivation in a thin-Cu(In, Ga)Se₂ solar cell, *Thin Solid Films*. 669 (2019) 399–403. doi:10.1016/j.tsf.2018.11.027.
- [14] S. Choi, Y. Kamikawa, J. Nishinaga, A. Yamada, H. Shibata, S. Niki, Lithographic fabrication of point contact with Al₂O₃ rear-surface-passivated and ultra-thin Cu(In,Ga)Se₂ solar cells, *Thin Solid Films*. 665 (2018) 91–95. doi:10.1016/j.tsf.2018.08.044.
- [15] J. van Deelen, M. Barink, L. Klerk, P. Voorthuijzen, A. Hovestad, Efficiency loss prevention in monolithically integrated thin film solar cells by improved front contact, *Prog. Photovolt. Res. Appl.* 23 (2015) 498–506. doi:10.1002/pip.2459.
- [16] G. Yin, A. Steigert, P. Manley, R. Klenk, M. Schmid, Enhanced absorption in tandem solar cells by applying hydrogenated In₂O₃ as electrode, *Appl. Phys. Lett.* 107 (2015) 211901. doi:10.1063/1.4936328.
- [17] J. van Deelen, Y. Tezsevin, M. Barink, Multi-Material Front Contact for 19% Thin Film Solar Cells, *Mater. Basel Switz.* 9 (2016). doi:10.3390/ma9020096.
- [18] T. Song, J.T. McGoffin, J.R. Sites, Interface-Barrier-Induced J–V Distortion of CIGS Cells With Sputtered-Deposited Zn(S,O) Window Layers, *IEEE J. Photovolt.* 4 (2014) 942–947. doi:10.1109/JPHOTOV.2014.2301894.
- [19] T. Minemoto, Y. Hashimoto, T. Satoh, T. Negami, H. Takakura, Y. Hamakawa, Cu(In,Ga)Se₂ solar cells with controlled conduction band offset of window/Cu(In,Ga)Se₂ layers, *J. Appl. Phys.* 89 (2001) 8327–8330. doi:10.1063/1.1366655.
- [20] H.-S. Bae, C. Kim, I. Rhee, H.-J. Jo, D.-H. Kim, S. Hong, Enhancement of the CIGS solar cell's efficiency by anti-reflection coating with Teflon AF, *J. Korean Phys. Soc.* 65 (2014) 1517–1519. doi:10.3938/jkps.65.1517.
- [21] Z.J. Li- Kao, N. Naghavi, F. Erfurth, J.F. Guillemoles, I. Gérard, A. Etcheberry, J.L. Pelouard, S. Collin, G. Voorwinden, D. Lincot, Towards ultrathin copper indium gallium diselenide solar cells: proof of concept study by chemical etching and gold back contact engineering, *Prog. Photovolt. Res. Appl.* 20 (2012) 582–587. doi:10.1002/pip.2162.
- [22] C. Onwudinanti, R. Vismara, O. Isabella, L. Grenet, F. Emieux, M. Zeman, Advanced light management based on periodic textures for Cu(In,Ga)Se₂ thin-film solar cells, *Opt. Express*. 24 (2016) A693–A707. doi:10.1364/OE.24.00A693.

- 1
2
3
4 [23] J. Krc, M. Sever, A. Campa, Z. Lokar, B. Lipovsek, M. Topic, Optical confinement in
5 chalcopyrite based solar cells, *Thin Solid Films*. 633 (2017) 193–201.
6 doi:10.1016/j.tsf.2016.08.056.
7
8 [24] J. Goffard, C. Colin, F. Mollica, A. Cattoni, C. Sauvan, P. Lalanne, J. Guillemoles, N.
9 Naghavi, S. Collin, Light Trapping in Ultrathin CIGS Solar Cells with Nanostructured Back
10 Mirrors, *IEEE J. Photovolt.* 7 (2017) 1433–1441. doi:10.1109/JPHOTOV.2017.2726566.
11
12 [25] N. Rezaei, O. Isabella, Z. Vroon, M. Zeman, Quenching Mo optical losses in CIGS solar
13 cells by a point contacted dual-layer dielectric spacer: a 3-D optical study, *Opt. Express*. 26
14 (2018) A39–A53. doi:10.1364/OE.26.000A39.
15
16 [26] G. Yin, A. Steigert, P. Andrae, M. Goebelt, M. Latzel, P. Manley, I. Lauer mann, S.
17 Christiansen, M. Schmid, Integration of plasmonic Ag nanoparticles as a back reflector in
18 ultra-thin Cu(In,Ga)Se₂ solar cells, *Appl. Surf. Sci.* 355 (2015) 800–804.
19 doi:10.1016/j.apsusc.2015.07.195.
20
21 [27] C. van Lare, G. Yin, A. Polman, M. Schmid, Light Coupling and Trapping in Ultrathin
22 Cu(In,Ga)Se₂ Solar Cells Using Dielectric Scattering Patterns, *ACS Nano*. 9 (2015) 9603–
23 9613. doi:10.1021/acs.nano.5b04091.
24
25 [28] B. Vermang, J.T. Watjen, V. Fjallstrom, F. Rostvall, M. Edoff, R. Gunnarsson, I. Pilch, U.
26 Helmersson, R. Kotipalli, F. Henry, D. Flandre, Highly reflective rear surface passivation
27 design for ultra-thin Cu(In,Ga) Se-2 solar cells, *Thin Solid Films*. 582 (2015) 300–303.
28 doi:10.1016/j.tsf.2014.10.050.
29
30 [29] M. Schmid, Review on light management by nanostructures in chalcopyrite solar cells,
31 *Semicond. Sci. Technol.* 32 (2017) 043003. doi:10.1088/1361-6641/aa59ee.
32
33 [30] J. Krc, F. Smole, M. Topic, One-dimensional semi-coherent optical model for thin film solar
34 cells with rough interfaces, *Inf. Midem-J. Microelectron. Electron. Compon. Mater.* 32
35 (2002) 6–13.
36
37 [31] J. Krč, M. Zeman, F. Smole, M. Topič, Optical modeling of a-Si:H solar cells deposited on
38 textured glass/SnO₂ substrates, *J. Appl. Phys.* 92 (2002) 749–755. doi:10.1063/1.1487910.
39
40 [32] J. Krč, F. Smole, M. Topič, Analysis of light scattering in amorphous Si:H solar cells by a
41 one-dimensional semi-coherent optical model, *Prog. Photovolt. Res. Appl.* 11 (2003) 15–26.
42 doi:10.1002/pip.460.
43
44 [33] B. Lipovsek, J. Krc, M. Topic, Optical Model for Thin-Film Photovoltaic Devices with
45 Large Surface Textures at the Front Side, *Inf. Midem-J. Microelectron. Electron. Compon.*
46 *Mater.* 41 (2011) 264–271.
47
48 [34] M. Sever, B. Lipovšek, J. Krč, A. Čampa, G. Sánchez Plaza, F.-J. Haug, M. Duchamp, W.
49 Soppe, M. Topič, Combined model of non-conformal layer growth for accurate optical
50 simulation of thin-film silicon solar cells, *Sol. Energy Mater. Sol. Cells*. 119 (2013) 59–66.
51 doi:10.1016/j.solmat.2013.05.016.
52
53 [35] C.K. Carniglia, Scalar Scattering Theory for Multilayer Optical Coatings, *Opt. Eng.* 18
54 (1979) 182104. doi:10.1117/12.7972335.
55
56 [36] P. Beckmann, A. Spizzichino, The Scattering of Electromagnetic Waves from Rough
57 Surfaces, Artech House, 1987.
58
59 [37] The COMSOL® Software Product Suite, COMSOL Multiphysics©. (n.d.).
60 <https://www.comsol.com/products> (accessed January 15, 2019).
61
62 [38] J.-M. Jin, The Finite Element Method in Electromagnetics, Wiley, 2002.
63
64 [39] A. Campa, J. Krc, M. Topic, Two Approaches for Incoherent Propagation of Light in
65 Rigorous Numerical Simulations, *Prog. Electromagn. Res.* 137 (2013) 187–202.
doi:10.2528/PIER13010407.

- 1
2
3
4 [40] M. Sever, J. Krč, M. Topič, Prediction of defective regions in optimisation of surface
5 textures in thin-film silicon solar cells using combined model of layer growth, *Thin Solid*
6 *Films*. 573 (2014) 176–184. doi:10.1016/j.tsf.2014.11.053.
7
8 [41] J.S. Orfanidis, *Electromagnetic Waves and Antennas*, Rutgers University, 2010.
9 www.ece.rutgers.edu/~orfanidi/ewa.
10 [42] J. Krc, G. Cernivec, A. Campa, J. Malmström, M. Edoff, F. Smole, M. Topic, Optical and
11 electrical modeling of Cu(In,Ga)Se₂ solar cells, *Opt. Quantum Electron.* 38 (2006) 1115–
12 1123. doi:10.1007/s11082-006-9049-1.
13 [43] R. Kotipalli, O. Poncelet, G. Li, Y. Zeng, L.A. Francis, B. Vermang, D. Flandre, Addressing
14 the impact of rear surface passivation mechanisms on ultra-thin Cu(In,Ga)Se-2 solar cell
15 performances using SCAPS 1-D model, *Sol. Energy*. 157 (2017) 603–613.
16 doi:10.1016/j.solener.2017.08.055.
17 [44] R. Kotipalli, B. Vermang, J. Joel, R. Rajkumar, M. Edoff, D. Flandre, Investigating the
18 electronic properties of Al₂O₃/Cu(In, Ga)Se-2 interface, *AIP Adv.* 5 (2015) 107101.
19 doi:10.1063/1.4932512.
20 [45] O. Lundberg, M. Bodegård, J. Malmström, L. Stolt, Influence of the Cu(In,Ga)Se₂ thickness
21 and Ga grading on solar cell performance, *Prog. Photovolt. Res. Appl.* 11 (2003) 77–88.
22 doi:10.1002/pip.462.
23 [46] refractiveindex.info, RefractiveIndex.INFO. (n.d.).
24 https://refractiveindex.info/?shelf=main&book=Al2O3&page=Malitson-o (accessed January
25 24, 2019).
26 [47] Y.-C. Lin, Y.-T. Hsieh, C.-M. Lai, H.-R. Hsu, Impact of Mo barrier layer on the formation
27 of MoSe₂ in Cu(In,Ga)Se₂ solar cells, *J. Alloys Compd.* 661 (2016) 168–175.
28 doi:10.1016/j.jallcom.2015.11.194.
29 [48] J. Krc, J. Malmström, F. Smole, M. Topic, Determination of light scattering properties of
30 Cu(In, Ga)Se₂ films for solar cells, *Proc 20th Eur. Photovolt. Sol. Energy Conf.* (2005)
31 1831–1834.
32 [49] J. Escarré, K. Söderström, C. Battaglia, F.-J. Haug, C. Ballif, High fidelity transfer of
33 nanometric random textures by UV embossing for thin film solar cells applications, *Sol.*
34 *Energy Mater. Sol. Cells.* 95 (2011) 881–886. doi:10.1016/j.solmat.2010.11.010.
35 [50] M. Meier, U.W. Paetzold, M. Prömpers, T. Merdzhanova, R. Carius, A. Gordijn, UV
36 nanoimprint for the replication of etched ZnO:Al textures applied in thin-film silicon solar
37 cells, *Prog. Photovolt. Res. Appl.* 22 (2014) 1226–1236. doi:10.1002/pip.2382.
38 [51] B. Lipovšek, J. Krč, M. Topič, Microtextured Light-Management Foils and Their
39 Optimization for Planar Organic and Perovskite Solar Cells, *IEEE J. Photovolt. PP* (2018)
40 1–10. doi:10.1109/JPHOTOV.2018.2810844.
41 [52] S. Albrecht, M. Saliba, J.P.C. Baena, F. Lang, L. Kegelman, M. Mews, L. Steier, A. Abate,
42 J. Rappich, L. Korte, R. Schlattmann, M.K. Nazeeruddin, A. Hagfeldt, M. Grätzel, B. Rech,
43 Monolithic perovskite/silicon-heterojunction tandem solar cells processed at low
44 temperature, *Energy Environ. Sci.* 9 (2016) 81–88. doi:10.1039/C5EE02965A.
45 [53] S. Esiner, T. Bus, M.M. Wienk, K. Hermans, R.A.J. Janssen, Quantification and Validation
46 of the Efficiency Enhancement Reached by Application of a Retroreflective Light Trapping
47 Texture on a Polymer Solar Cell, *Adv. Energy Mater.* 3 (2013) 1013–1017.
48 doi:10.1002/aenm.201300227.
49 [54] C. Ulbrich, A. Gerber, K. Hermans, A. Lambert, U. Rau, Analysis of short circuit current
50 gains by an anti-reflective textured cover on silicon thin film solar cells, *Prog. Photovolt.*
51 *Res. Appl.* 21 (2013) 1672–1681. doi:10.1002/pip.2249.
52
53
54
55
56
57
58
59
60
61
62
63
64
65